Pergamon

Int. J. Heat Mass Transfer. Vol. 38, No. 10, pp. 1911–1921, 1995

0017-9310/95 $9.50+0.00

0017-9310(94)00238-X

The effects of $SiCl_4$ and $GeCl_4$ oxidation, variable properties, buoyancy and tube rotation on the modified chemical vapor deposition process

S. JOH† and R. GREIF‡

Department of Mechanical Engineering, University of California at Berkeley, Berkeley, CA 94720, U.S.A.

(*Received* 20 *December* 1993 *and in final form* 15 *July* 1994)

Abstract—A study is made of the flow, heat and mass transfer, particle formation and deposition, including the $SiCl_4$ and $GeCl_4$ oxidation reactions and the effects of buoyancy, variable properties and tube rotation with application to the modified chemical vapor deposition (MCVD) process. The steady-state three-dimensional governing conservation equations, which include the continuity, species, momentum and energy equations have been solved numerically. The resulting temperature, velocity and species concentration fields permit the determination of the particle formation and particle deposition efficiencies. Of special interest are the effects of the chemical reactions on particle formation and deposition.

INTRODUCTION

The modified chemical vapor deposition (MCVD) process is widely used for the manufacture of high-quality optical fiber preforms [1–5]. In this process, a hollow silica tube is mounted in a lathe which is rotating about its axis. Reactant gases, e.g. $SiCl_4$, $GeCl_4$ and O_2 flow through the tube and are heated by a moving exterior torch which traverses back and forth along the tube. The gases are heated as they approach the torch; chemical reactions then take place and submicron particles, e.g. SiO_2 and GeO_2, are formed. Particles deposit due to thermophoresis on the inner surface of the tube, although some particles flow out of the tube without depositing.

In analyses of the MCVD process, several effects have been studied. Walker *et al.* [6] studied thermophoretic particle deposition in a two-dimensional variable property flow. The importance of buoyancy was studied in laser-enhanced MCVD processes by Wang *et al.* [7], DiGiovanni *et al.* [8] and Morse *et al.* [9]. The effects of thermal radiation on particle deposition were studied by Paz *et al.* [10] and Jia *et al.* [11]. Annulus MCVD was proposed and studied by Fiebig *et al.* [12]. Choi *et al.* [13] studied the effects of tube rotation and variable properties on the three-dimensional temperature field, particle trajectories and deposition for a fast moving torch. Choi *et al.* [14] analyzed the effects of tube rotation and localized torch heating using a fully developed velocity profile. The effects of variable properties, buoyancy and tube rotation were studied using a perturbation analysis [15]. Lin *et al.* [16] studied the effects of buoyancy, variable properties and tube rotation in a three-dimensional numerical analysis of the flow and heat transfer for the MCVD process. An analysis of particle deposition was also carried out with an assumed reaction temperature [17]. The effects of the solid layer were studied for constant properties by Lin *et al.* [18]. Park and Choi [19] studied the effects of the solid layer and periodic heating for the MCVD process. A two-torch system and the heat flux boundary condition are used to simulate the heating that occurs in the MCVD process.

A study of chemical kinetics and silica aerosol dynamics has been carried out by Kim and Pratsinis [20] with respect to the MCVD process. Kim and Pratsinis [21] solved the conservation equations and included the effects of variable properties and multiple chemical species ($SiCl_4$, $GeCl_4$) in a two-dimensional formulation. Joh *et al.* [22] solved the energy equation and species equations for the gas ($SiCl_4$) and the particles (SiO_2) in a two-dimensional study for fully developed flow in a tube. They showed, for low flow rates and high inlet $SiCl_4$ concentrations, that a rapid increase (spike) in the temperature of the gas occurs which alters the deposition characteristics. In view of the large temperature differences that are present in the MCVD process, it is important to include the effects of variable properties, buoyancy and chemical reactions in studies of the process. In this work the conservation equations are solved to obtain the three-dimensional velocity, species concentration and temperature profiles which permit the determination of the particle formation, particle deposition and total

† Present address: Computational Mechanics Department, Sandia National Laboratories, Livermore, CA 94550, U.S.A.

‡ Author to whom correspondence should be addressed.

NOMENCLATURE

$C_{GC,in}$ inlet gas ($GeCl_4$) concentration [mol cm^{-3}]
$C_{SC,in}$ inlet gas ($SiCl_4$) concentration [mol cm^{-3}]
c_p heat capacity of O_2 [J g^{-1} K^{-1}]
D_{Cl} diffusivity of Cl_2 in O_2 [cm^2 s^{-1}]
D_{GC} diffusivity of $GeCl_4$ in O_2 [cm^2 s^{-1}]
D_{GO} diffusivity of GeO_2 in O_2 [cm^2 s^{-1}]
D_{O_2} diffusivity of O_2 [cm^2 s^{-1}]
D_{SC} diffusivity of $SiCl_4$ in O_2 [cm^2 s^{-1}]
D_{SO} diffusivity of SiO_2 in O_2 [cm^2 s^{-1}]
E_{GC} activation energy for $GeCl_4$ oxidation [kJ mol^{-1}]
E_{PD} percentage of particle deposition
E_{PF} percentage of particle formation
E_{SC} activation energy for $SiCl_4$ oxidation [kJ mol^{-1}]
E_T total deposition efficiency
g gravitational acceleration [m s^{-2}]
ΔH_{GC} enthalpy of the reaction for $GeCl_4$ oxidation [kJ mol^{-1}]
ΔH_{SC} enthalpy of the reaction for $SiCl_4$ oxidation [kJ mol^{-1}]
K thermophoretic coefficient
K_{eq} equilibrium constant for $GeCl_4$ oxidation
k thermal conductivity of O_2 [W m^{-1} K^{-1}]
$k_{GC,0}$ pre-exponential Arrhenius rate constant [cm^3 mol^{-1} s^{-1}]
$k_{SC,1}$ pre-exponential Arrhenius rate constant [cm^3 mol^{-1} s^{-1}]
$k_{SC,0}$ pre-exponential Arrhenius rate constant [s^{-1}]
L length of the tube [m]
L_t distance between the torch and the specified inlet [m]
$\bar{M}$ average molecular weight of the gases
M_{Cl} molecular weight of Cl_2
M_{GC} molecular weight of $GeCl_4$
M_{GO} molecular weight of GeO_2
M_{O_2} molecular weight of O_2
M_{SC} molecular weight of $SiCl_4$
M_{SO} molecular weight of SiO_2
Q inlet flow rate [l min^{-1}]
R gas constant
r radial coordinate [m]
r_{GC} reaction rate for $GeCl_4$ oxidation
r_{SC} reaction rate for $SiCl_4$ oxidation
T temperature [K]
T_{in} temperature at the inlet plane
T_{max} maximum temperature on the tube wall
T_{rxn} reaction temperature
T_w wall temperature
t time [s]
U_{avg} average velocity of gas in the axial direction [m s^{-1}]
U_T torch speed [m s^{-1}]
u axial velocity (in the steady-state reference coordinate system) [m s^{-1}]
u_T thermophoretic velocity in the axial direction [m s^{-1}]
v radial velocity [m s^{-1}]
v_T thermophoretic velocity in the radial direction [m s^{-1}]
$\overline{v_T}$ average radial thermophoretic velocity over the angular direction [m s^{-1}]
w circumferential velocity [m s^{-1}]
w_T thermophoretic velocity in the angular direction [m s^{-1}]
X_{O_2} mole fraction of O_2 in the gas phase
x axial coordinate [m s^{-1}]
Y_{Cl} mass fraction of Cl_2 in the gas phase
Y_{GC} mass fraction of $GeCl_4$ in the gas phase
Y_{GO} mass fraction of GeO_2 in the solid phase
Y_{O_2} mass fraction of O_2 in the gas phase
Y_{SC} mass fraction of $SiCl_4$ in the gas phase
Y_{SO} mass fraction of SiO_2 in the solid phase.

Greek symbols

γ sticking coefficient
θ angle
μ dynamic viscosity [kg m^{-1} s^{-1}]
ν kinematic viscosity [cm^2 s^{-1}]
ξ moving coordinate, $x - U_T t$
ρ density [kg m^{-3}]
Ω angular velocity of tube [rpm].

Subscripts

Cl Cl_2
GC $GeCl_4$
GO GeO_2
in inlet
PD particle deposition
PF particle formation
r radial coordinate
SC $SiCl_4$
SO SiO_2
w wall
ξ moving coordinate, $x - U_T t$.

Superscript

$\bar{}$ average.

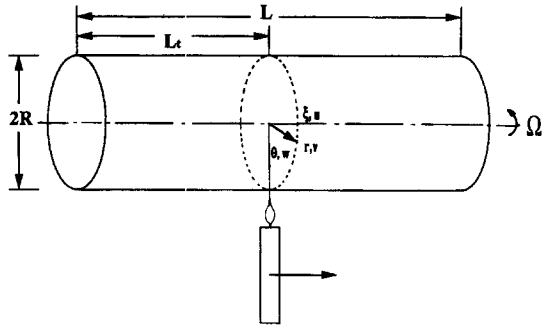

Fig. 1. Sketch of the system.

deposition efficiencies for both the silica and the germanium particles. The parameters include the inlet gas concentrations, inlet flow rate, tube rotation rate, torch speed and wall temperature.

ANALYSIS

The reactant gases, $SiCl_4$, $GeCl_4$ and O_2, flow in a tube that is rotating about its axis. The tube is heated by a torch and the gases react to form silica (SiO_2) and germanium (GeO_2) particles and chlorine (Cl_2) gas. The particles are transported by convection, diffusion and thermophoresis.

Governing equations

The introduction of the coordinates $\xi = x - U_T t$, θ, and r results in the quasi-steady-state system shown in Fig. 1. The governing equations for the three-dimensional laminar flow, including the effects of chemical reactions, variable properties and buoyancy (the viscous dissipation and pressure work terms in the energy equation are assumed to be negligible) are:

continuity,

$$\frac{1}{r}\frac{\partial(r\rho v)}{\partial r}+\frac{1}{r}\frac{\partial(\rho w)}{\partial\theta}+\frac{\partial(\rho u)}{\partial\xi}=0 \tag{1}$$

momentum,

$$\rho v\frac{\partial u}{\partial r}+\rho\frac{w}{r}\frac{\partial u}{\partial\theta}+\rho(u-U_T)\frac{\partial u}{\partial\xi}=-\frac{\partial p}{\partial\xi}+\nabla\cdot(\mu\nabla u) \tag{2}$$

$$\rho v\frac{\partial v}{\partial r}+\rho\frac{w}{r}\frac{\partial v}{\partial\theta}+\rho(u-U_T)\frac{\partial v}{\partial\xi}-\rho\frac{w^2}{r}$$
$$=-\frac{\partial p}{\partial r}+\rho g\cos\theta+\nabla\cdot(\mu\nabla v)-\mu\frac{v}{r^2}-\mu\frac{2}{r^2}\frac{\partial w}{\partial\theta} \tag{3}$$

$$\rho v\frac{\partial w}{\partial r}+\rho\frac{w}{r}\frac{\partial w}{\partial\theta}+\rho(u-U_T)\frac{\partial w}{\partial\xi}+\rho\frac{vw}{r}$$
$$=-\frac{1}{r}\frac{\partial p}{\partial\theta}-\rho g\sin\theta+\nabla\cdot(\mu\nabla w)-\mu\frac{w}{r^2}\frac{\partial v}{\partial\theta} \tag{4}$$

energy,

$$\rho c_P v\frac{\partial T}{\partial r}+\rho c_P\frac{w}{r}\frac{\partial T}{\partial\theta}+\rho c_P(u-U_T)\frac{\partial T}{\partial\xi}$$
$$=\nabla\cdot(k\nabla T)+\Delta H_{SC}r_{SC}+\Delta H_{GC}r_{GC} \tag{5}$$

species equations for $SiCl_4$ (SC), $GeCl_4$ (GC), Cl_2 (Cl) and O_2 gases,

$$\rho v\frac{\partial Y_{SC}}{\partial r}+\rho\frac{w}{r}\frac{\partial Y_{SC}}{\partial\theta}+\rho(u-U_T)\frac{\partial Y_{SC}}{\partial\xi}$$
$$=\nabla\cdot(\rho D_{SC}\nabla Y_{SC})-r_{SC} \tag{6}$$

$$\rho v\frac{\partial Y_{GC}}{\partial r}+\rho\frac{w}{r}\frac{\partial Y_{GC}}{\partial\theta}+\rho(u-U_T)\frac{\partial Y_{GC}}{\partial\xi}$$
$$=\nabla\cdot(\rho D_{GC}\nabla Y_{GC})-r_{GC} \tag{7}$$

$$\rho v\frac{\partial Y_{Cl}}{\partial r}+\rho\frac{w}{r}\frac{\partial Y_{Cl}}{\partial\theta}+\rho(u-U_T)\frac{\partial Y_{Cl}}{\partial\xi}$$
$$=\nabla\cdot(\rho D_{Cl}\nabla Y_{Cl})+2r_{SC}\frac{M_{Cl}}{M_{SC}}+2r_{GC}\frac{M_{Cl}}{M_{GC}} \tag{8}$$

$$\rho v\frac{\partial Y_{O_2}}{\partial r}+\rho\frac{w}{r}\frac{\partial Y_{O_2}}{\partial\theta}+\rho(u-U_T)\frac{\partial Y_{O_2}}{\partial\xi}$$
$$=\nabla\cdot(\rho D_{O_2}\nabla Y_{O_2})-r_{SC}\frac{M_{O_2}}{M_{SC}}-r_{GC}\frac{M_{O_2}}{M_{GC}} \tag{9}$$

species equations for SiO_2 (SO) and GeO_2 (GO) particles,

$$\rho v\frac{\partial Y_{SO}}{\partial r}+\rho\frac{w}{r}\frac{\partial Y_{SO}}{\partial\theta}+\rho(u-U_T)\frac{\partial Y_{SO}}{\partial\xi}$$
$$=\nabla\cdot(\rho D_{SO}\nabla Y_{SO})-\frac{1}{r}\frac{\partial}{\partial r}(r\rho Y_{SO}v_T)-\frac{\partial}{\partial\xi}(\rho Y_{SO}w_T)$$
$$-\frac{1}{r}\frac{\partial(\rho Y_{SO}u_T)}{\partial\theta}+r_{SC}\frac{M_{SO}}{M_{SC}} \tag{10}$$

$$\rho v\frac{\partial Y_{GO}}{\partial r}+\rho\frac{w}{r}\frac{\partial Y_{GO}}{\partial\theta}+\rho(u-U_T)\frac{\partial Y_{GO}}{\partial\xi}$$
$$=\nabla\cdot(\rho D_{GO}\nabla Y_{GO})-\frac{1}{r}\frac{\partial}{\partial r}(r\rho Y_{GO}v_T)-\frac{\partial}{\partial\xi}(\rho Y_{GO}u_T)$$
$$-\frac{1}{r}\frac{\partial(\rho Y_{GO}w_T)}{\partial\theta}+r_{GC}\frac{M_{GO}}{M_{GC}} \tag{11}$$

$$u_T=-\frac{Kv}{T}\frac{\partial T}{\partial\xi}w_T=-\frac{Kv}{T}\frac{1}{r}\frac{\partial T}{\partial\theta}v_T=-\frac{Kv}{T}\frac{\partial T}{\partial r} \tag{12}$$

where K, the thermophoretic coefficient, is 0.55 [20, 23].

The chemical reaction rates are included by using single-step global reactions with Arrhenius rates; i.e.

$$SiCl_4(g)+O_2(g)\longrightarrow SiO_2(s)+2Cl_2(g)$$
$$r_{SC}=\left(k_{SC,0}+k_{SC,1}\frac{\rho Y_{O_2}}{M_{O_2}}\right)e^{-E_{SC}/RT}\frac{\rho Y_{SC}}{M_{SC}} \tag{13}$$

$$GeCl_4(g)+O_2(g)\longleftrightarrow GeO_2(s)+2Cl_2(g)$$
$$r_{GC}=k_{GC,0}\,e^{-E_{GC}/RT}\rho^2\left(\frac{Y_{GC}Y_{O_2}}{M_{GC}M_{O_2}}-\frac{\gamma Y_{GO}Y_{Cl}^2}{K_{eq}M_{Cl}^2}\right)\ln K_{eq}$$
$$=-98.33-2.2525\times10^{-3}T+\frac{19\,690}{T}+12.01\ln T \tag{14}$$

where $k_{SC,0}$, $k_{SC,1}$ and $k_{GC,0}$ are specified by Kim and Pratsinis [21]. The density, thermal conductivity, viscosity and diffusivity are calculated for the carrier gas O_2 [24–26]. The density ρ is obtained from the ideal gas law, i.e.

$$\rho = \frac{p\bar{M}}{RT}.$$

Boundary conditions

The distance L is the length of the tube and L_t is the distance between the inlet and the torch. The boundary conditions are:

$$\text{at } r = R, \quad w = R\Omega, \quad v = 0, \quad u = 0$$

$$T_W = (T_{max} - T_I)\frac{(L_t + \xi)}{L_t} + T_I \quad \text{for} \quad -L_t \leqslant \xi \leqslant 0$$

$$T_W = (T_{max} - T_I)\exp[-(\lambda\xi)^2] + T_I \quad \text{for} \quad \xi > 0$$

$$\frac{\partial Y_{SC}}{\partial r} = \frac{\partial Y_{GC}}{\partial r} = \frac{\partial Y_{Cl}}{\partial r} = \frac{\partial Y_{O_2}}{\partial r} = \frac{\partial Y_{SO}}{\partial r} = \frac{\partial Y_{GO}}{\partial r} = 0$$

at $r = 0$, u, v, w, T, Y_{SC}, Y_{GC}, Y_{O_2}, Y_{Cl}, Y_{SO}, Y_{GO} are finite;

$$\text{at } \xi = -L_t, \quad w = r\Omega, \quad v = 0$$

$$u = 2V_{av}\left(1 - \frac{r^2}{R^2}\right) - U_T, \quad T = T_I$$

$$Y_{SC} = Y_{SC,I}, \quad Y_{GC} = Y_{GC,I}, \quad Y_{O_2} = Y_{O_2,I}$$

$$Y_{Cl} = Y_{SO} = Y_{GO} = 0. \tag{15}$$

The wall temperature is based on the measurements of Walker *et al.* [6, 27], increases linearly behind the torch and decreases exponentially ahead of the torch. The torch is located at $\xi = 0$. At the entrance, $\xi = -L_t$, the temperature is equal to a constant value, T_I; here the axial component of velocity is given by the fully developed Poiseuille velocity profile, the angular component of velocity varies linearly with respect to the radius, and there is no radial component of velocity. Calculations were carried out for two conditions at the outlet boundary; i.e. for the first or for the second derivatives in the streamwise direction of the dependent variables being set equal to zero. The results for the two outlet conditions are virtually identical.

NUMERICAL PROCEDURE

The governing partial differential equations are nonlinear and coupled. An iterative numerical procedure was employed to solve for the velocity, temperature and species fields. The computer code that was used is based on the TEACH code of Gosman and Ideriah [28] (cf. Lavine [29], Goering [30] and Lin [31]). The continuity, momentum, energy and species equations were solved simultaneously to obtain the primitive variables.

A staggered grid arrangement similar to the MAC grid of Harlow and Welsh [32] is used where the main grid nodes are the storage locations for the pressure and the other scalar quantities. The velocity components are located at points midway between the main grid nodes on the main node interfaces. A staggered grid minimizes the problems of oscillatory pressure and velocity fields which arise when non-staggered grids are utilized [33, 34].

The normalized residues of the velocities, temperature, pressure and species concentrations were summed over all of the control volumes. The iterations were continued until the normalized residuals and the relative changes of the dependent variables were less than 0.1%.

Calculations were made for different grid sizes for both uniform and nonuniform grids. The results for a $22 \times 11 \times 100$ uniform grid differed by less than 1% from $33 \times 22 \times 100$ and from $22 \times 11 \times 150$ grids at several locations near and down stream from the torch. The SIMPLER [35] iteration procedure has a slower convergence rate for nonuniform grids; the results for the nonuniform grids were essentially the same as for the uniform grids and the $22 \times 11 \times 100$ uniform grid was used in these calculations. Additional information is also given in Joh *et al.* [22]. The typical CPU time needed to obtain convergent solutions is more than 8 h on a CRAY Y-MP computer.

Table 1. The range of the conditions in the MCVD process

Inlet gas concentrations	3.0×10^{-6} mol cm^{-3} ($SiCl_4$) 1.9×10^{-6} mol cm^{-3} ($GeCl_4$)
Flow rate	1–5 l min^{-1}
Maximum wall temperature	1873, 2173 K
Tube radius	0.01 m
Tube length	0.6 m
Inlet temperature	300 K
Tube rotation	0, 60 rpm
Torch speed	20 cm min^{-1} (T_{max} = 1873 K) 10 cm min^{-1} (T_{max} = 2173 K)

RESULTS AND DISCUSSION

Calculations were carried out over the range of conditions that are listed in Table 1. The properties were evaluated for oxygen which is the dominant species ($X_{O_2} \approx 0.9$) and are given in Table 2. The acti-

Table 2. Properties of the carrier gas (O_2)†

$(\mu/\rho) = \nu = \nu_0 T^{1.64374}$	$\nu_0 = 1.39 \times 10^{-5}$
$k = k_0 + k_1 T + k_2 T^2$	$k_0 = 1.08 \times 10^{-5}$
$D_{SC} = D_{SC,0} T^{1.6561}$	$k_1 = 1.82 \times 10^{-7}$
$D_{GC} = D_{GC,0} T^{1.6561}$	$k_2 = -2.34 \times 10^{-11}$
$D_{SO} = D_{SO,0} T^{1.6561}$	$D_{SC,0} = 6.32 \times 10^{-6}$
$D_{GO} = D_{GO,0} T^{1.6561}$	$D_{GC,0} = 6.0 \times 10^{-6}$
$D_{O_2} = D_{O_2,0} T^{1.6561}$	$D_{O_2,0} = 1.76 \times 10^{-5}$
$D_{Cl} = D_{Cl,0} T^{1.6561}$	$D_{Cl,0} = 1.12 \times 10^{-5}$
$c_p = 1.09$ J g^{-1} K^{-1}	$D_{SO,0} = 1.0 \times 10^{-10}$
	$D_{GO,0} = 1.0 \times 10^{-10}$

† T (K), ν (cm^2 s^{-1}), k (W cm^{-1} K^{-1}), D (cm^2 s^{-1}).

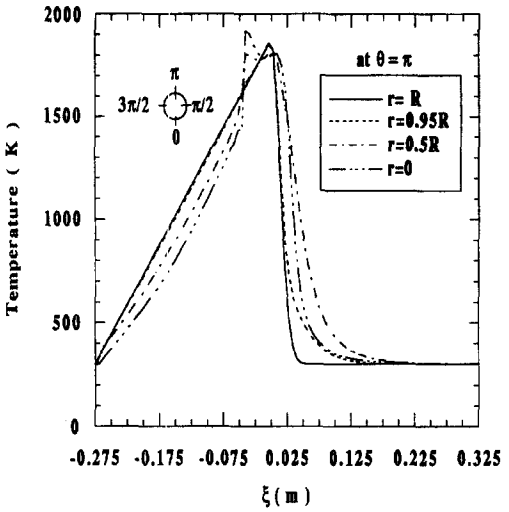

Fig. 2. Axial distribution of wall and gas temperature in the upper diameter ($\theta = \pi$).

vation energies, E, for $SiCl_4$ and for $GeCl_4$, were 402 and 263 kJ mol^{-1}, respectively; the reaction enthalpies, ΔH, for $SiCl_4$ and for $GeCl_4$, were 251 and 46 kJ mol^{-1}, respectively, and the pre-exponential factors, $k_{SC,0}$, $k_{SC,1}$ and $k_{GC,0}$, were 1.7×10^{14} s^{-1}, 3.1×10^{19} and 2.3×10^{15} cm^3 mol^{-1} s^{-1} [21]. The conditions selected are based on simulations of the manufacture of light-guide preforms [3, 6, 36]. A total length, L, of 0.6 m was used along with $L_t = 0.275$ and 0.3 m.

The conditions $\Omega = 60$ rpm, $Q = 11$ min^{-1} (for carrier gas O_2 and dilute gases, $SiCl_4$ and $GeCl_4$), $T_{max} = 1873$ K, $U_T = 20$ cm min^{-1}, $SiCl_4$ flow rate = 0.51 g min^{-1} ($C_{SC,0} = 3 \times 10^{-6}$ mol cm^{-3}) and $GeCl_4$ flow rate = 0.4 g min^{-1} ($C_{GC,0} = 1.89 \times 10^{-6}$ mol cm^{-3}) are first studied. The axial temperature variations at different radial locations are shown in Fig. 2. There is a region behind the torch where there is a rapid increase (spike) in the temperature of the gas due to the release of energy from the oxidation reactions, and the gas temperature becomes greater than the surrounding wall temperature. The gas temperature then decreases and becomes less than the wall temperature. In the region ahead of the torch, $\xi > 0$, the wall temperature decreases rapidly; the gas temperature also decreases, but again becomes higher than the surrounding wall temperature. Figure 3(a) and (b) shows the isothermal contours on the vertical and horizontal diameters. The increasing gas temperature (decreasing density) in the axial direction causes the gas to accelerate from the entrance to the region near the torch; the gas then decelerates as the temperature decreases [cf. Fig. 4(a) and (b)].

A secondary flow results from the effects of tube rotation and buoyancy [cf. Fig. 5(a), $\xi = -0.162$ m, which is behind the torch]. Note that in the center of the tube the cooler gas flowing downward [Fig. 5(a)] results in colder temperatures over the bottom half of the tube [Fig. 3(a)].

In the region ahead of the torch the gas is at a higher temperature than the surrounding cold wall; the effects of buoyancy are pronounced and influence the flow over the entire cross-section [e.g. $\xi = 0.034$ m, Fig. 5(b)]. Here the upward secondary flow results in higher temperatures over the top half of the tube [Fig. 3(a)]. The upward flow aids deposition over the upper half of the tube, but opposes deposition over the lower half; this contributes to nonuniform particle deposition [e.g. see Figs. 5(d) and 6(b)].

Figure 7(a) and (b) shows the axial variations of the species concentrations along the vertical radius for the gases ($SiCl_4$, $GeCl_4$) and for the particles (SiO_2, GeO_2). Figure 8 shows the results for E_{PF}, the particle formation (reaction conversion) efficiency, and, for E_T, the total particle deposition efficiency, for both oxidation reactions.

As the temperature increases downstream, the $GeCl_4$ reaction is initiated (near the wall) and the GeO_2 concentration increases [Figs. 7(b) and 8]. The temperature continues to increase and the $SiCl_4$ reaction then becomes important [$\xi \approx -0.05$, Fig. 7(a)] and considerable energy is released (as noted previously). Both reactions then occur over a greater portion of the tube cross-section [Fig. 7(a) and (b)]. Note that complete depletion of $SiCl_4$ occurs; i.e. $SiCl_4$ oxidation is complete with 100% particle formation (Fig. 8); $GeCl_4$, however, is present at all axial locations (Fig. 8). Over the interval -0.05 m $< \xi < 0.00$ the $GeCl_4$ reaction is diminished; in this region the gas temperature is increasing (> 1800 K) and the concentration of $GeCl_4$ increases while that of GeO_2 decreases [the equilibrium constant for $GeCl_4$ oxidation, K_{eq}, decreases with temperature (equation 14)]. The conversion of $SiCl_4$ to SiO_2, E_{PF}, is 100%, while the conversion of $GeCl_4$ to GeO_2 is only 45%; the total deposition efficiency, E_T, for $SiCl_4$ is 61% and for $GeCl_4$ is 30% (Fig. 8). The spike causes high temperatures to occur behind the torch; i.e. at an axial location before the maximum wall temperature, T_{max}, is reached [Figs. 2 and 3(a)]. This causes some deposition to occur behind the torch, but most of the deposition occurs downstream of the torch (Fig. 8).

The axial variation of the radial thermophoretic velocity, v_T, at and near the tube surface on the upper vertical radius ($r = R$ and $0.95R$) are shown in Fig. 6(a). Positive values of v_T are velocities toward the wall and are present both behind and ahead of the torch; the positive values ahead of the torch (where most of the deposition takes place) are much larger than the values behind the torch. The variation in the circumferential direction of the radial thermophoretic velocity, v_T, at the surface is seen in Fig. 6(b), and is due primarily to buoyancy. The magnitude of v_T is higher near the wall than near the center [Fig. 5(d)]. Near the center there is a strong secondary flow contribution which affects the particle motion [Fig. 5(b)].

The deposition depends on the wall temperature and the flow rate in a complex manner (see Table 3 for $T_{max} = 1873$ K). For low flow rates ($Q = 1$

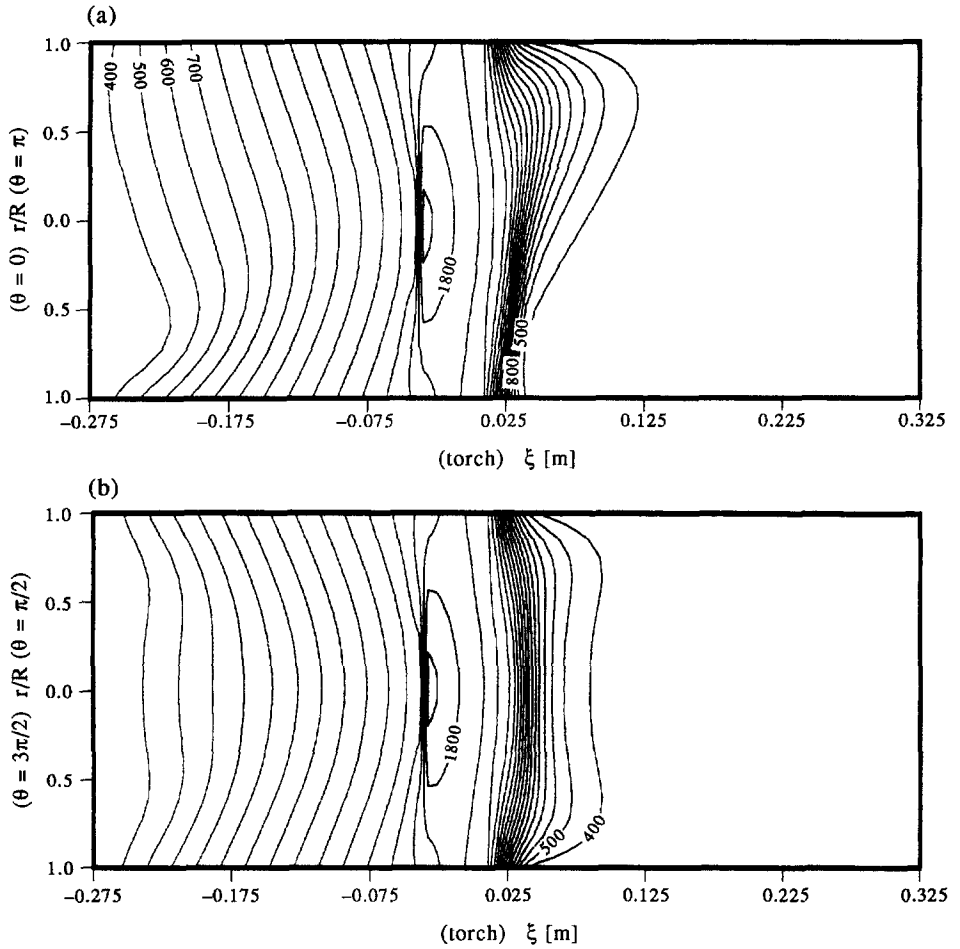

Fig. 3. (a) Isothermal contours in the central vertical plane: $\Omega = 60$ rpm, $Q = 1$ l min^{-1}, $T_{max} = 1873$ K, $C_{in}(SiCl_4) = 3.0 \times 10^{-6}$ mol cm^{-3}, $C_{in}(GeCl_4) = 1.89 \times 10^{-6}$ mol cm^{-3}, $U_T = 20$ cm min^{-1}. (b) Isothermal contours in the central horizontal plane: $\Omega = 60$ rpm, $Q = 1$ l min^{-1}, $T_{max} = 1873$ K, $C_{in}(SiCl_4) = 3.0 \times 10^{-6}$ mol cm^{-3}, $C_{in}(GeCl_4) = 1.89 \times 10^{-6}$ mol cm^{-3}, $U_T = 20$ cm min^{-1}.

l min^{-1}), the higher gas temperatures behind the torch result in a large value of the conversion of $SiCl_4$ gas to particles (SiO_2), E_{PF} is 100% but E_{PD} is 61%; for high flow rates ($Q = 5$ l min^{-1}), E_{PF} is only 37% and E_{PD} is 89%. For GeO_2, at $Q = 1$ l min^{-1}, E_{PF} is 45% and E_{PD} is 67%; at $Q = 5$ l min^{-1}, E_{PF} is 24% and E_{PD} is 83%. For $Q = 1$ l min^{-1} the low value of the particle deposition efficiency, E_{PD}, is due primarily to the fact that particles are formed over the entire cross-section of the tube and those particles that are formed near the tube center pass out of the tube; i.e. do not deposit. For high flow rates ($Q = 5$ l min^{-1}) the gas temperature is lower in the region behind the torch but higher in the region far ahead of the torch, and the reactions to form SiO_2 and GeO_2 only take place in a small region very close to the wall, near the torch location, and thus a greater fraction of the particles are deposited (i.e. E_{PD} is high). Another consideration is related to the radial temperature gradient ahead of the torch, where there is a rapidly cooling wall (and where most of the deposition takes place). Although the gas is hotter behind the torch for $Q = 1$ than for 5 l min^{-1}, the rapidly cooling wall ahead of the torch dramatically cools the gas for the slower flow rate; the result is that the thermophoretic velocity, v_T, at the wall (e.g. at $\theta = \pi$, $\xi = 0.022$ m) is smaller for $Q = 1$ l min^{-1} ($v_T = 0.015$ m s^{-1}) than it is for $Q = 5$ l min^{-1} ($v_T = 0.029$ m s^{-1}). The total deposition efficiency for SiO_2, $E_T = E_{PF} \times E_{PD}$, is 61% for $Q = 1$ l min^{-1}, but is only 33% for $Q = 5$ l min^{-1}; for GeO_2, E_T is 30% for $Q = 1$ l min^{-1} and 20% for $Q = 5$ l min^{-1}.

At the higher temperature, $T_{max} = 2173$ K, and for $Q = 1$ l min^{-1}, E_{PF} for SiO_2 is 100%, $E_{PD} = 57\%$, $E_T = 57\%$ and E_{PF} for GeO_2 is 40%, $E_{PD} = 63\%$, $E_T = 25\%$; for $Q = 5$ l min^{-1}, E_{PF} for SiO_2 is 91%, $E_{PD} = 68\%$, $E_T = 61\%$ and E_{PF} for GeO_2 is 40%, $E_{PD} = 65\%$ and $E_T = 26\%$. The higher temperature causes $SiCl_4$ oxidation to be complete but $GeCl_4$ oxidation is not complete (on the contrary E_{PF} for GeO_2 is lower than for $T_{max} = 1873$ K because of the importance of the reverse $GeCl_4$ oxidation reaction at higher

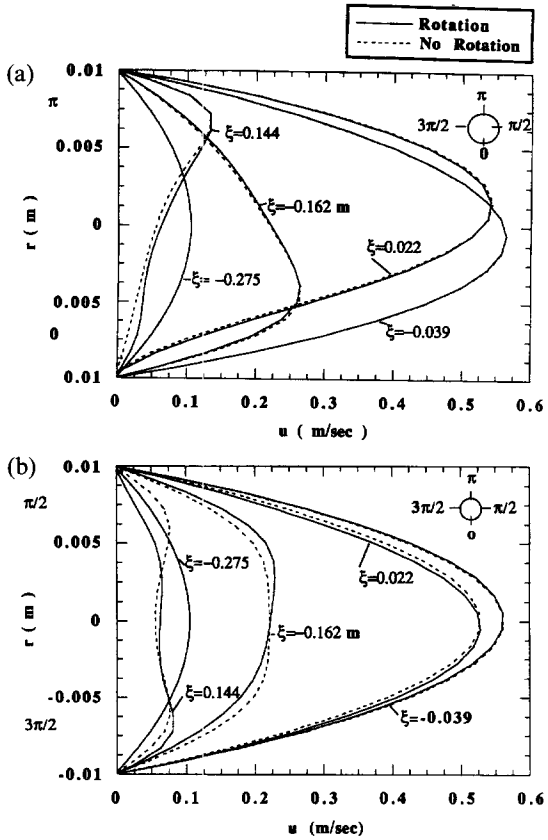

Fig. 4. (a) Axial velocity component distribution along the vertical diameter at different axial locations for variable properties: $\Omega = 0$ rpm (dot line), $\Omega = 60$ rpm (solid line), $Q = 1$ l min^{-1}, $T_{max} = 1873$ K, $C_{in}(SiCl_4) = 3.0 \times 10^{-6}$ mol cm^{-3}, $C_{in}(GeCl_4) = 1.89 \times 10^{-6}$ mol cm^{-3}, $U_T = 20$ cm min^{-1}. (b) Axial velocity component distribution along the horizontal diameter at different axial locations for variable properties: $\Omega = 0$ rpm (dot line), $\Omega = 60$ rpm (solid line), $Q = 1$ l min^{-1}, $T_{max} = 1873$ K, $C_{in}(SiCl_4) = 3.0 \times 10^{-6}$ mol cm^{-3}, $C_{in}(GeCl_4) = 1.89 \times 10^{-6}$ mol cm^{-3}, $U_T = 20$ cm min^{-1}.

temperature). Note that at high gas temperatures, both GeO_2 and Cl_2 will dissociate, but these effects are not considered in this study.

At $Q = 1$ l min^{-1}, for SiO_2 there is a smaller value for E_T (57%) at $T_{max} = 2173$ K than (61%) at 1873 K. For $Q = 1$ l min^{-1} both temperatures result in similar regions where there is particle formation (behind the torch) and $E_{PF} = 100\%$ (for SiO_2). For $T_{max} = 2173$ K, the axial velocities are larger (than for 1873 K), due to the smaller density and more particles pass out of the tube (smaller E_{PD} of 57% and smaller E_T of 57% for $T_{max} = 2173$ K). For $T_{max} = 2173$ K and $Q = 5$ l min^{-1}, a high value of E_{PF} of 89% (more particles are formed due to the high gas temperatures) results in the higher value of E_T of 61% (vs E_{PF} of 37% and E_T of 33% at 1873 K).

At $Q = 3$ l min^{-1} both $T_{max} = 1873$ and 2173 K give $E_{PF} = 100\%$ and high values of E_T of 66% and 65% for $SiCl_4$ and 32 and 28% for $GeCl_4$, respectively. For $Q = 3$ l min^{-1} the reactions occur not only in the region behind the torch, but also ahead of the torch, which results in high values of E_{PF} and E_T. The important deposition region ahead of the torch is enhanced due to the chemical heat release in this region; this causes the gas temperature to increase and results in the higher radial thermophoretic velocity; e.g. $\overline{v_T}$, the average value of v_T over the angular direction, is 0.026 m s^{-1} for 1873 K and $\overline{v_T} = 0.031$ m s^{-1} for 2173 K at $\xi = 0.022$ m and $r = R$ (vs $\overline{v_T} = 0.017$ m s^{-1} for 1873 K and $\overline{v_T} = 0.019$ m s^{-1} for 2173 K at $Q = 1$ l min^{-1}). For both temperatures and for both $Q = 1$ and 3 l min^{-1}, $E_{PF} = 100\%$ for SiO_2; for 1873 K E_T is 61 and 66% for $Q = 1$ and 3 l min^{-1}, respectively. Note that E_T for $Q = 3$ l min^{-1} is greater than for $Q = 1$ l min^{-1}. The higher value of E_T is related to the location of the particle formation. For $Q = 1$ l min^{-1} the $SiCl_4$ oxidation reaction begins (and is completed) behind the torch and the heat release from the reaction results in a spike behind the torch. However, for $Q = 3$ l min^{-1} the $SiCl_4$ oxidation reaction also starts behind the torch, but now continues ahead of the torch (the higher flow rate results in lower gas temperatures behind the torch). For $Q = 3$ l min^{-1} the $SiCl_4$ oxidation reaction behind the torch takes place near the wall, but ahead of the torch the reaction takes place near the tube center (and not near the wall). In front of the torch the cold wall causes the radial temperature gradient to be large and the secondary flow due to the variable properties and buoyancy is important.

The above results include the effects of buoyancy, variable properties and rotation. The additional transport from buoyancy causes particles to form over the entire cross-section; when buoyancy is omitted the particles form only near the wall and not in the center. The values of E_{PF} and E_T are higher with buoyancy than without buoyancy (Tables 3 and 4). For low flow rates ($Q = 1$ l min^{-1}) E_{PF} for $SiCl_4$ at 1873 K is the same (100%) with and without buoyancy, but E_T is 61 and 48% with and without buoyancy, respectively. For moderate flow rates ($Q = 3$ l min^{-1}) E_{PF} for $SiCl_4$ at 1873 K is still 100% with buoyancy, but 68% without buoyancy; E_T is 66 and 57%, respectively. For high flow rates ($Q = 5$ l min^{-1}) E_{PF} for $SiCl_4$ at 1873 K is 37 and 32% with and without buoyancy; E_T is 33 and 31% with and without buoyancy, respectively. The trends for E_{PF} and E_T with and without buoyancy for $T_{max} = 2173$ K are similar to the results for 1873 K. Note that, as the flow rate increases, the effects of buoyancy decrease.

The interaction of rotation, buoyancy and axial convection results in complex velocity fields. For moderate rotational speeds, e.g. $\Omega = 60$ rpm (cf. Simpkins *et al.* [3]), the axial velocity distributions along the vertical and horizontal diameters differ only slightly from the non-rotating condition [Fig. 4(a) and (b)]. Behind the torch the gas flows upward (due to buoyancy) around the hot wall and then downward in the cold central region; ahead of the torch the gas flows downward around the cold wall and upward in the hot center. [This is true with rotation (60 rpm) and

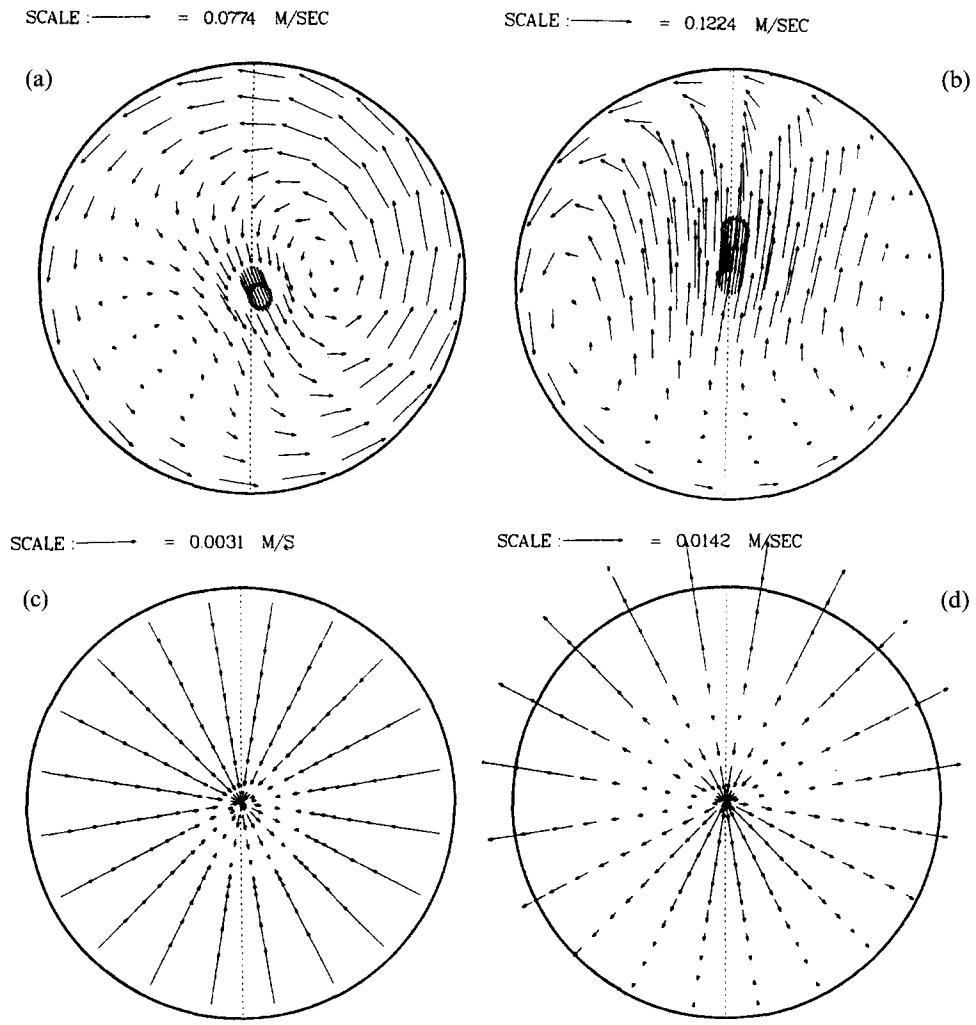

Fig. 5. Secondary flow pattern for variable properties and buoyancy with rotation: (a) at $\xi = -0.162$ m; (b) at $\xi = 0.034$ m; $\Omega = 60$ rpm, $Q = 1\ 1\ \text{min}^{-1}$, $T_{max} = 1873$ K, $C_{in}(SiCl_4) = 3.0 \times 10^{-6}$ mol cm^{-3}, $C_{in}(GeCl_4) = 1.89 \times 10^{-6}$ mol cm^{-3}, $U_T = 20$ cm min^{-1}. Distribution of radial thermophoretic velocity for variable properties and buoyancy: (c) at $\xi = -0.162$ m; (d) at $\xi = 0.034$ m; $\Omega = 60$ rpm, $Q = 1\ 1\ \text{min}^{-1}$, $T_{max} = 1873$ K, $C_{in}(SiCl_4) = 3.0 \times 10^{-6}$ mol cm^{-3}, $C_{in}(GeCl_4) = 1.89 \times 10^{-6}$ mol cm^{-3}, $U_T = 20$ cm min^{-1}.

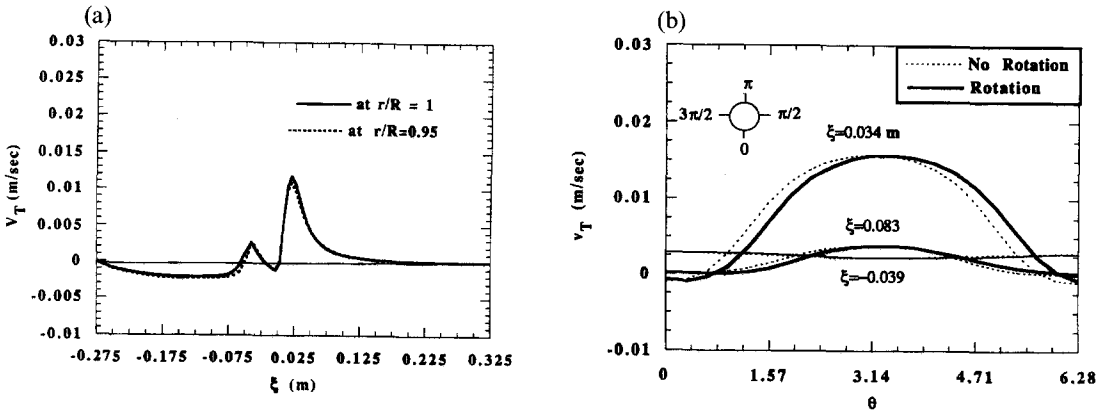

Fig. 6. (a) Axial distribution of radial thermophoretic velocity at $r/R = 1$ and $r/R = 0.95$ ($\theta = \pi$): $\Omega = 60$ rpm, $Q = 1\ 1\ \text{min}^{-1}$, $T_{max} = 1873$ K, $C_{in}(SiCl_4) = 3.0 \times 10^{-6}$ mol cm^{-3}, $C_{in}(GeCl_4) = 1.89 \times 10^{-6}$ mol cm^{-3}, $U_T = 20$ cm min^{-1}. (b) Angular distribution of radial thermophoretic velocity on the wall at different axial locations: $\Omega = 60$ rpm, $Q = 1\ 1\ \text{min}^{-1}$, $T_{max} = 1873$ K, $C_{in}(SiCl_4) = 3.0 \times 10^{-6}$ mol cm^{-3}, $C_{in}(GeCl_4) = 1.89 \times 10^{-6}$ mol cm^{-3}, $U_T = 20$ cm min^{-1}.

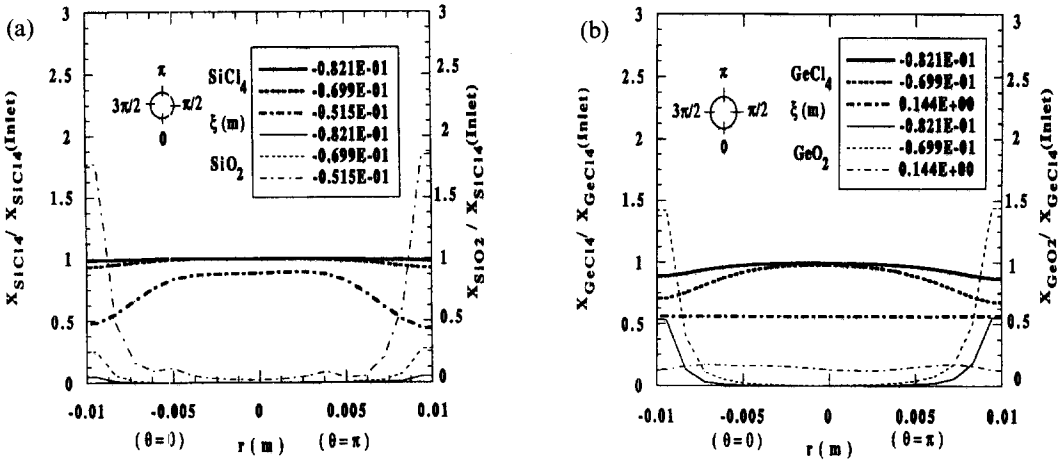

Fig. 7. (a) Distribution of dimensionless concentrations of $SiCl_4$ and SiO_2 along the central vertical diameter at different axial locations: $\Omega = 60$ rpm, $Q = 1$ l min^{-1}, $T_{max} = 1873$ K, $C_{in}(SiCl_4) = 3.0 \times 10^{-6}$ mol cm^{-3}, $C_{in}(GeCl_4) = 1.89 \times 10^{-6}$ mol cm^{-3}, $U_T = 20$ cm min^{-1}. (b) Distribution of dimensionless concentrations of $GeCl_4$ and GeO_2 along the central vertical diameter at different axial locations: $\Omega = 60$ rpm, $Q = 1$ l min^{-1}, $T_{max} = 1873$ K, $C_{in}(SiCl_4) = 3.0 \times 10^{-6}$ mol cm^{-3}, $C_{in}(GeCl_4) = 1.89 \times 10^{-6}$ mol cm^{-3}, $U_T = 20$ cm min^{-1}.

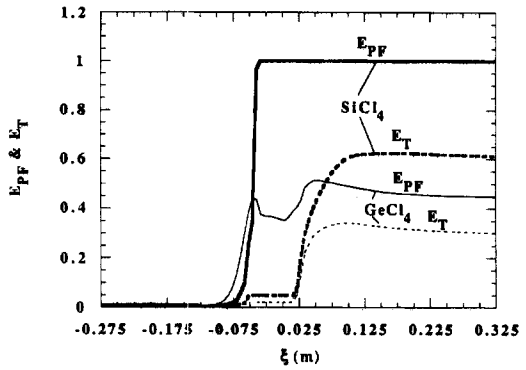

Fig. 8. Spatial variation of percentage of particle formation, $E_{PF}(\xi)$, and total deposition efficiency, $E_T(\xi)$, for $SiCl_4$ and $GeCl_4$: $\Omega = 60$ rpm, $Q = 1$ l min^{-1}, $T_{max} = 1873$ K, $C_{in}(SiCl_4) = 3.0 \times 10^{-6}$ mol cm^{-3}, $C_{in}(GeCl_4) = 1.89 \times 10^{-6}$ mol cm^{-3}, $U_T = 20$ cm min^{-1}.

Table 3. The particle formation efficiency (E_{PF}), particle deposition efficiency (E_{PD}) and total deposition efficiency ($E_T = E_{PF} \times E_{PD}$) for $T_{max} = 1873$ K

	Q (l min^{-1})	$T_{max} = 1873$ K, $C_{in}(SiCl_4) = 3.0 \times 10^{-6}$, $C_{in}(GeCl_4) = 1.89 \times 10^{-6}$ mol cm^{-3} Buoyancy $SiCl_4$	Buoyancy $GeCl_4$	No buoyancy $SiCl_4$	No buoyancy $GeCl_4$
E_{PF}	1	100%	45%	100%	45%
E_{PD}		61%	67%	48%	58%
E_T		61%	30%	48%	26%
E_{PF}	3	100%	45%	68%	39%
E_{PD}		66%	71%	84%	72%
E_T		66%	32%	57%	28%
E_{PF}	5	37%	24%	32%	20%
E_{PD}		89%	83%	97%	95%
E_T		33%	20%	31%	19%

Table 4. The particle formation efficiency (E_{PF}), particle deposition efficiency (E_{PD}) and total deposition efficiency ($E_T = E_{PF} \times E_{PD}$) for $T_{max} = 2173$ K

	Q (l min^{-1})	$T_{max} = 2173$ K, $C_{in}(SiCl_4) = 3.0 \times 10^{-6}$, $C_{in}(GeCl_4) = 1.89 \times 10^{-6}$ mol cm^{-3} Buoyancy $SiCl_4$	Buoyancy $GeCl_4$	No buoyancy $SiCl_4$	No buoyancy $GeCl_4$
E_{PF}	1	100%	40%	100%	38%
E_{PD}		57%	63%	41%	53%
E_T		57%	25%	41%	20%
E_{PF}	3	100%	43%	100%	39%
E_{PD}		65%	65%	56%	56%
E_T		65%	28%	56%	22%
E_{PF}	5	89%	40%	66%	31%
E_{PD}		69%	65%	85%	71%
E_T		61%	26%	56%	22%

without rotation.] Near the torch, the strong secondary radial flow pattern due to buoyancy is dominant and is present with rotation [$\Omega = 60$ rpm, Fig. 5(b)] and without rotation ($\Omega = 0$, not shown). Also note the variation of the radial thermophoretic velocity in the circumferential direction with and without rotation [Fig. 6(b)].

For a nonrotating system, the resulting velocity, temperature and concentration fields are symmetric with respect to the vertical diameter; with rotation present the contours are not symmetric. However, with a rotational speed of $\Omega = 60$ rpm, the distributions of temperature, velocity and species concentrations differ only slightly from those without rotation. The values of E_{PF}, E_{PD} and E_T are the same with rotation ($\Omega = 60$ rpm) and without rotation (Tables 3 and 4); thus, a tube rotation of 60 rpm does not change the total results for particle formation and deposition in respect to the nonrotating condition.

SUMMARY AND CONCLUSIONS

A study has been made of the flow, heat and mass transfer relative to the MCVD process. Numerical solutions for the three-dimensional velocity, temperature and species concentrations have been obtained, including the effects of chemical reactions, variable properties, buoyancy and tube rotation. The efficiency of the conversion of the gases ($SiCl_4$, $GeCl_4$) to particles (SiO_2, GeO_2), E_{PF}, the efficiency of particle deposition, E_{PD}, and the total deposition efficiency, E_T, have been determined. The following conclusions are drawn.

(1) The effects of variable properties result in a significant change in the axial variation of the axial component of velocity due primarily to the change in density. Buoyancy results in a strong upward secondary flow in the region near the torch which aids particle deposition over the upper portion of the tube. Buoyancy results in a nonuniform circumferential gas temperature distribution which causes a variation of the thermophoretic force. Thermophoresis is dominant near the wall but is less important in the central region of the tube.

(2) For the range of parameters studied most of the deposition takes place ahead of the torch where the wall temperature is low.

(3) A spike in the gas temperature profile occurs for low flow rate, $Q = 1\ l\ min^{-1}$, and high inlet $SiCl_4$ concentration, $C_{in}(SiCl_4) = 3.0 \times 10^{-6}$ mol cm^{-3}, for both $T_{max} = 1873$ and 2173 K. The spike causes some deposition to take place behind the torch.

(4) For low flow rate ($Q = 1\ l\ min^{-1}$) and for both wall temperature cases ($T_{max} = 1873$ and 2173 K), SiO_2 and GeO_2 particles are formed over the entire tube cross-section. For the formation of SiO_2 particles, E_{PF} is 100%, E_{PD} is 61 and 57%, and E_T is 61 and 57%, for 1873 and 2173 K, respectively. For GeO_2 particles, E_{PF} is only 45 and 40%, E_{PD} is 67 and 63%, and E_T is 30 and 25%, for 1873 and 2173 K, respectively.

(5) For a flow rate of $Q = 3\ l\ min^{-1}$ and both $T_{max} = 1873$ and 2173 K cases, SiO_2 and GeO_2 particles are formed over the entire tube cross-section near the torch. For SiO_2, E_{PF} is 100%, E_{PD} is 66 and 65% and E_T is 66 and 65% for 1873 and 2173 K; for GeO_2, E_{PF} is 45 and 43%, E_{PD} is 71 and 65% and E_T is 32 and 28% for 1873 and 2173 K, respectively. Note that this flow rate of $Q = 3\ l\ min^{-1}$ gives high values of E_{PD} (in comparison to $Q = 1\ l\ min^{-1}$) because reactions take place behind and also ahead of the torch; this results in high gas temperatures and large radial thermophoretic velocities over a larger region.

(6) A high flow rate ($Q = 5\ l\ min^{-1}$) results in lower temperatures and for $T_{max} = 1873$ K yields, for SiO_2, a low E_{PF} of 37%, a high E_{PD} of 89%, and an E_T of 33%; for GeO_2 E_{PF} is 24%, E_{PD} is 83%, and E_T is 20%. For $T_{max} = 2173$ K, for SiO_2 E_{PF} is 89%, E_{PD} is 69%, E_T is 61%, and for GeO_2 E_{PF} is 40%, E_{PD} is 65% and E_T is 26%. There is no spike in the gas temperature profiles at the higher flow rates.

(7) $GeCl_4$ oxidation is not complete for any of the conditions studied, due to the importance of the reverse reaction at high temperatures ($T > 1800$ K); E_{PF} varies from 25 to 45% for the different cases studied.

(8) Buoyancy results in higher values of E_{PF} and E_T. The effects of buoyancy are more pronounced for lower flow rates ($Q = 1\ l\ min^{-1}$).

(9) A tube rotation of 60 rpm has little effect on E_{PF}, E_{PD} and E_T.

Acknowledgements—Support from the National Science Foundation, the Pittsburgh Supercomputer Center and the University of California Computing Center is gratefully acknowledged. The research is part of a joint program with Professor J. W. Daily of the University of Colorado on chemical vapor deposition processes.

REFERENCES

1. J. B. MacChesney, P. B. O'Connor, F. V. DiMarcello, J. R. Simpson and P. D. Lazay, Preparational low-loss optical fibers using simultaneous vapor phase deposition and fusion, *Proceedings of the 10th International Congress on Glass*, Kyoto, Japan, pp. 6-40–6-44 (1974).
2. J. B. MacChesney, P. B. O'Connor and H. M. Presby, A new technique for preparation of low-loss and graded index optical fibers, *Proc. IEEE* **62,** 1278–1279 (1974).
3. P. G. Simpkins, S. G. Kosinski and J. B. MacChesney, Thermophoresis: the mass transfer mechanism in modified chemical vapor deposition, *J. Appl. Phys.* **50,** 5676–5681 (1979).
4. K. L. Walker, G. M. Homsy and F. T. Geyling, Thermophoretic deposition of small particles in laminar tube flow, *J. Colloid Interface Sci.* **69,** 138–147 (1979).
5. S. R. Nagel, J. B. MacChesney and K. L. Walker, An overview of the modified chemical vapor deposition (MCVD) process and performance, *IEEE J. Quantum Electron.* **QE-18**(4), 459–476 (1982).
6. K. L. Walker, F. T. Geyling and S. R. Nagel, Thermophoretic deposition of small particles in the modified chemical vapor deposition (MCVD) process, *J. Am. Ceram. Soc.* **63,** 552–558 (1980).
7. C. Y. Wang, T. F. Morse and J. W. Cipolla Jr, Laser induced natural convection and thermophoresis, *ASME J. Heat Transfer* **107,** 161–167 (1985).
8. D. DiGiovanni, C. Y. Wang, T. F. Morse and J. W. Cipolla Jr, Laser induced buoyancy and forced convection in vertical tubes. In *Natural Convection: Fundamentals and Applications* (Edited by S. Kakac, W. Aung and R. Viskanta), pp. 1118–1139. Hemisphere, New York (1985).
9. T. F. Morse, D. DiGiovanni, Y. W. Chen and J. W. Cipolla Jr, Laser enhancement of thermophoretic deposition process, *J. Lightwave Technol.* **LT-4**(2), 151–155 (1986).
10. L. P. Paz, J. W. Cipolla Jr and T. F. Morse, The effects of radiation on particle deposition in MCVD: the optically thin case, *HTP* **106,** 157–162 (1989).
11. G. Jia, Y. Yerner and J. W. Cipolla Jr, Thermophoresis of a reacting aerosol in thermally developing Poiseuille flow, *Int. J. Heat Mass Transfer* **35,** 3265–3273 (1992).
12. M. Fiebig, M. Hilgenstock and H.-A. Riemann, The modified chemical vapor deposition process in a concentric annulus, *Aerosol Sci. Technol.* **9,** 237–249 (1988).
13. M. Choi, H. R. Baum and R. Greif, The heat transfer problem during the modified chemical vapor deposition process, *ASME J. Heat Transfer* **109,** 642–646 (1987).

14. M. Choi, R. Greif and H. R. Baum, A study of heat transfer and particle motion relative to the modified chemical vapor deposition process, *ASME J. Heat Transfer* **111,** 1031–1037 (1989).
15. M. Choi, Y. T. Lin and R. Greif, Analysis of buoyancy and tube rotation relative to the modified chemical vapor deposition process, *ASME J. Heat Transfer* **112,** 1063–1069 (1990).
16. Y. T. Lin, M. Choi and R. Greif, A three dimensional analysis of the flow and heat transfer for the modified chemical vapor deposition process including buoyancy, variable properties and tube rotation, *ASME J. Heat Transfer* **113,** 400–406 (1991).
17. Y. T. Lin, M. Choi and R. Greif, A three dimensional analysis of particle deposition for the modified chemical vapor deposition (MCVD) process, *ASME J. Heat Transfer* **114,** 735–742 (1992).
18. Y. T. Lin, M. Choi and R. Greif, An analysis of the effect of solid layer for the modified chemical vapor deposition process, *Warme- und Stoffubertragung* **28,** 169–176 (1993).
19. K. S. Park and M. Choi, Conjugate heat transfer and particle deposition in the modified chemical vapor deposition process: effects of torch speed and solid layer, Submitted.
20. K. S. Kim and S. E. Pratsinis, Manufacture of optical waveguide preforms by modified chemical vapor deposition, *A.I.Ch.E. Jl* **34,** 912–920 (1988).
21. K. S. Kim and S. E. Pratsinis, Codeposition of SiO_2/GeO_2 during production of optical fiber preforms by modified chemical vapor deposition, *Int. J. Heat Mass Transfer* **33,** 1977–1986 (1990).
22. S. Joh, R. Greif and Y. S. Lin, A study of the effects of chemical reaction on the MCVD process, *J. Mater. Process. Manuf. Sci.* **1,** 369–386 (1993).
23. L. Talbot, R. K. Cheng, R. W. Schefer and D. R. Willis, Thermophoresis of particles in a heated boundary layer, *J. Fluid Mech.* **101,** Pt 4, 737–758 (1980).
24. R. C. Weast and M. J. Astle, *CRC Handbook of Chemistry and Physics* (61st Edn). CRC Press, Boca Raton, FL (1981).
25. R. H. Perry and D. Green, *Perry's Chemical Engineers' Handbook* (6th Edn). McGraw-Hill, New York (1984).
26. R. C. Reid, J. M. Prausnitz and T. K. Sherwood, *The Properties of Gases and Liquids* (3rd Edn). McGraw-Hill, New York (1977).
27. K. L. Walker, Personal communication, AT&T Bell Laboratories, Murray Hill, NJ (1992).
28. A. D. Gosman and J. F. K. Ideriah, *TEACH-2E: a General Computer Program for Two-dimensional, Turbulent, Recirculating Flows.* Imperial College, London (1976).
29. A. G. Lavine, A three-dimensional analysis of natural convection in a toroidal loop, Ph.D. Thesis, University of California, Berkeley, CA (1984).
30. D. J. Goering, The influence of curvature and buoyancy in three-dimensional pipe flows, Ph.D. Thesis, University of California, Berkeley, CA (1989).
31. Y. T. Lin, Studies of flow, heat transfer and particle deposition during chemical vapor deposition, Ph.D. Thesis, University of California, Berkeley, CA (1991).
32. F. H. Harlow and J. E. Welsh, Numerical calculation of time dependent viscous incompressible flow of fluid with a free surface, *Phys. Fluids* **8,** 2182–2189 (1965).
33. S. V. Patankar, *Numerical Heat Transfer and Fluid Flows.* Hemisphere, New York (1980).
34. R. Peyret and T. D. Taylor, *Computational Methods for Fluid Flow.* Springer-Verlag, New York (1983).
35. S. V. Patankar, A calculation procedure for two-dimensional elliptic situations, *Numer. Heat Transfer* **2** (1979).
36. D. L. Wood, K. L. Walker, J. B. MacChesney, J. R. Simpson and R. Csencsits, Germanium chemistry in the MCVD process for optical fiber fabrication, *J. Lightwave Technol.* **LT-5,** 277–285 (1987).